Electrochemistry Communications 54 (2015) 18–22

Contents lists available at ScienceDirect

Electrochemistry Communications

journal homepage: www.elsevier.com/locate/elecom

Short communication

Ether-based electrolyte enabled Na/FeS_2 rechargeable batteries

Yujie Zhu, Liumin Suo, Tao Gao, Xiulin Fan, Fudong Han, Chunsheng Wang *

Department of Chemical and Biomolecular Engineering, University of Maryland, College Park, MD 20742, USA

ARTICLE INFO

Article history:
Received 26 January 2015
Received in revised form 8 February 2015
Accepted 8 February 2015
Available online 28 February 2015

Keywords:
Sodium ion batteries
Cathode
FeS_2
Electrolyte

ABSTRACT

We demonstrate for the first time that by simply substituting ether-based electrolyte (1.0 M $NaCF_3SO_3$ in diglyme) for the commonly used carbonate-based electrolyte, the cyclability of FeS_2 towards sodium storage can be significantly improved. A sodiation capacity over 600 mAh/g and a discharge energy density higher than 750 Wh/kg are obtained for FeS_2 at 20 mA/g. When tested at 60 mA/g, FeS_2 presents a sodiation capacity of 530 mAh/g and retains 450 mAh/g after 100 cycles, much better than the cycling performance of Na/FeS_2 tested in carbonate-based electrolyte.

1. Introduction

Recently, sodium ion batteries have been realized as an alternative to lithium ion batteries for large-scale energy storage applications due to the low cost of sodium [1,2]. In recent years, various high capacity anode materials have been developed for sodium ion batteries [3–8]. However, on the cathode side, the capacity is often low (<200 mAh/g), mainly due to the intrinsic limit of intercalation-type cathodes, which can only accommodate one Na^+ per transition metal core [9]. Alternative chemistries with higher capacities arise from conversion-reaction type materials, benefiting from their ability of accommodating more than one sodium ion per transition metal core. Among all conversion-reaction type materials, FeS_2, which is a well-known semiconductor for photovoltaic applications [10], is very cheap, naturally abundant, and environmentally benign. Indeed, FeS_2 has been used by *Energizer* in high capacity primary Li/FeS_2 batteries [11] and several groups have recently reported the successful development of rechargeable Li/FeS_2 batteries with excellent electrochemical performance [12–15]. FeS_2 can provide a high theoretical capacity of ~894 mAh/g (based on $FeS_2 + 4Na = Fe + 2Na_2S$), more than four times higher than the capacity of intercalation-type materials. The high capacity along with the very cheap raw materials makes Na/FeS_2 system a very promising low cost energy storage system. So far, there are only few reports for Na/FeS_2 system in the literature. Almost all of them showed unsatisfactory electrochemical performance with poor reversibility and fast capacity degradation during cycling [16,17]. Recent studies by Okada et al. [18] and Fu et al. [19] indicated that the reaction mechanism between sodium and FeS_2 is complicated and intermediate sodium polysulfide might be involved, as suggested by Ahn et al. [16] based on the phase diagram of sodium–sulfur. If intermediate sodium polysulfide is generated during the sodiation/desodiation of FeS_2, it is expected to react with carbonate-based electrolyte similar to the reaction between soluble lithium polysulfide and carbonate-based electrolyte via a nucleophilic addition or substitution, which will generate thio-carbonates as nicely demonstrated by Yim et al. [20]. Thus, carbonate-base electrolytes obviously are not a smart choice for Na/FeS_2 system.

Here, for the first time, we demonstrate that by simply substituting ether-based electrolyte for the commonly used carbonate-based electrolyte, the cyclability of FeS_2 towards sodium storage can be significantly enhanced. A sodiation capacity over 600 mAh/g and a discharge energy density higher than 750 Wh/kg can be obtained for FeS_2 at 20 mA/g. When tested at 60 mA/g, FeS_2 presents a sodiation capacity of 530 mAh/g and retains 450 mAh/g after 100 cycles, much better than the cycling performance of Na/FeS_2 tested in carbonate-based electrolyte and the Na/FeS_2 system reported in the literature.

2. Experimental

2.1. Synthesis of FeS_2

FeS_2 was prepared by a two-step method (Fig. 1a). First, Fe_3O_4/carbon composite was synthesized by an aerosol spray pyrolysis method [21]. Briefly, 3.2 g iron (III) nitrate nonahydrate ($Fe(NO_3)_3 \cdot 9H_2O$, Sigma-Aldrich) and 6.4 g sucrose ($C_{12}H_{22}O_{11}$, Sigma-Aldrich) were dissolved into 100 mL distilled water. The solution was nebulized into aerosol droplets, which were carried by argon gas and entered a tubular furnace pre-heated to 700 °C. The sample was collected at the end of the tubular furnace. Second, the Fe_3O_4/carbon composite was mixed with sulfur in a weight ratio of 1:2 and sealed in a glass tube under vacuum condition.

* Corresponding author. Tel.: +1 301 405 0352.
E-mail address: cswang@umd.edu (C. Wang).

http://dx.doi.org/10.1016/j.elecom.2015.02.006
1388-2481/

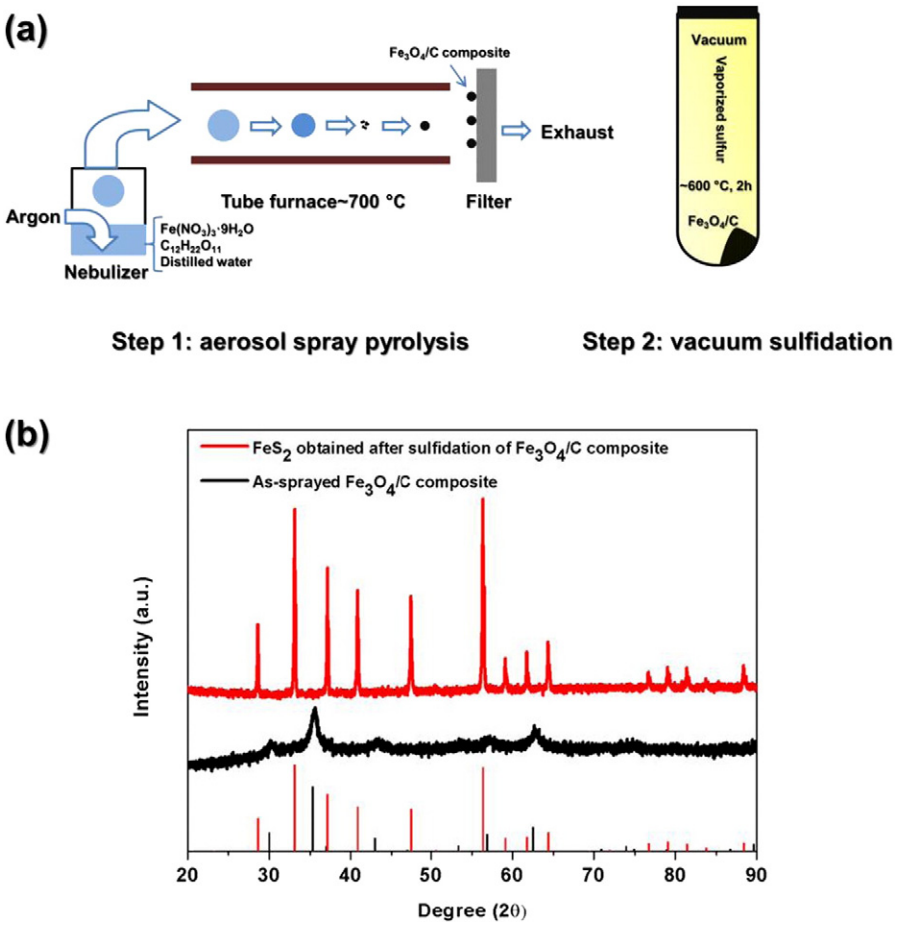

Fig. 1. (a) Schematic illustration of the synthesis process of FeS_2. (b) XRD patterns of as-sprayed Fe_3O_4/carbon composite and FeS_2 obtained from vacuum sulfidation of Fe_3O_4/carbon composite. The standard XRD patterns for Fe_3O_4 (JCPDS card no.: 99-0073) and FeS_2 (JCPDS card no.: 99-0087) are also plotted.

The glass tube was heated to 600 °C and held for 2 h. After the glass tube naturally cooled down, the powder was collected and washed with carbon disulfide to remove excess sulfur.

2.2. Material characterizations

The crystal structures of the samples were studied by powder X-ray diffraction (XRD) using a CuKα radiation source on a D8 Advanced with LynxEye and SolX (Bruker AXS, WI, USA) operated at 40 kV and 40 mA in the 2θ range of 10°–90°. Scanning electron microscope (SEM) and transmission electron microscope (TEM) were used to investigate the morphologies of the samples.

2.3. Electrochemical tests

The synthesized FeS_2 was manually mixed with sodium alginate binder in water and carbon black in a weight ratio of 85:10:5 to form slurry. Electrode was prepared by coating the slurry onto copper foil with a doctor blade. Then the electrode was dried in a vacuum oven under 100 °C for 5 h to remove water. The active material loading on the electrode was about 1.5–2.0 mg/cm^2. CR2032-type coin cells were assembled inside an argon-filled glove box. Sodium foil was used as the counter electrode, Celgard 3501 microporous film was chosen as the separator, and 1.0 M sodium triflate ($NaCF_3SO_3$, 98%, Sigma-Aldrich) in diglyme ($(CH_3OCH_2CH_2)_2O$, anhydrous, 99.5%, Sigma-Aldrich) was selected as the electrolyte for coin cell preparation. For comparison, coin cells with carbonate-based electrolyte (1.0 M $NaCF_3SO_3$ in ethylene carbonate (EC)/diethyl carbonate (DEC) with a volume ratio of 1:1) were also assembled and tested. Galvanostatic charge–discharge tests were performed on an Arbin battery test station (BT2000, Arbin Instruments, USA). Coin cells were cycled between 0.6 and 3 V (vs. Na/Na^+) under various current densities. Both current density and specific capacity were calculated on the basis of the weight of as-synthesized FeS_2 in the electrode.

3. Results and discussion

Fig. 1b shows the XRD patterns of the samples. The XRD peak intensity of the as-sprayed material is weak and these peaks can be indexed to Fe_3O_4, which was generated by incomplete thermal decomposition of $Fe(NO_3)_3 \cdot 9H_2O$ under an inert atmosphere. The weak peak intensity indicates a low degree of crystallinity, caused by the rapid heating and cooling during the aerosol spray process. After Fe_3O_4/carbon reacts with sulfur vapor under vacuum condition, the XRD pattern of the sample can be well indexed to FeS_2 with no crystalline impurity detected.

Fig. 2 shows the SEM and TEM images of Fe_3O_4/carbon composite and FeS_2. As shown in Fig. 2a and b, the Fe_3O_4/carbon composite has a well-defined spherical shape with a diameter around hundreds of nanometers. As evidenced by the contrast difference in the TEM images (Fig. 2c), the Fe_3O_4/carbon composite has a mesoporous/hollow structure [21]. High resolution TEM image (Fig. 2d) shows that Fe_3O_4 particles with a diameter less than 10 nm are embedded in the carbon matrix. It is hoped that this mesoporous structure could be preserved for FeS_2, which will be beneficial to its electrochemical performance. However, after sulfidation, the obtained FeS_2 presents an irregular shape (Fig. 2e and f). As shown by the TEM images in Fig. 2g and h, the diameter of the FeS_2 is in the range of 100–600 nm, much larger than that of Fe_3O_4 in the Fe_3O_4/carbon composite and indicating the

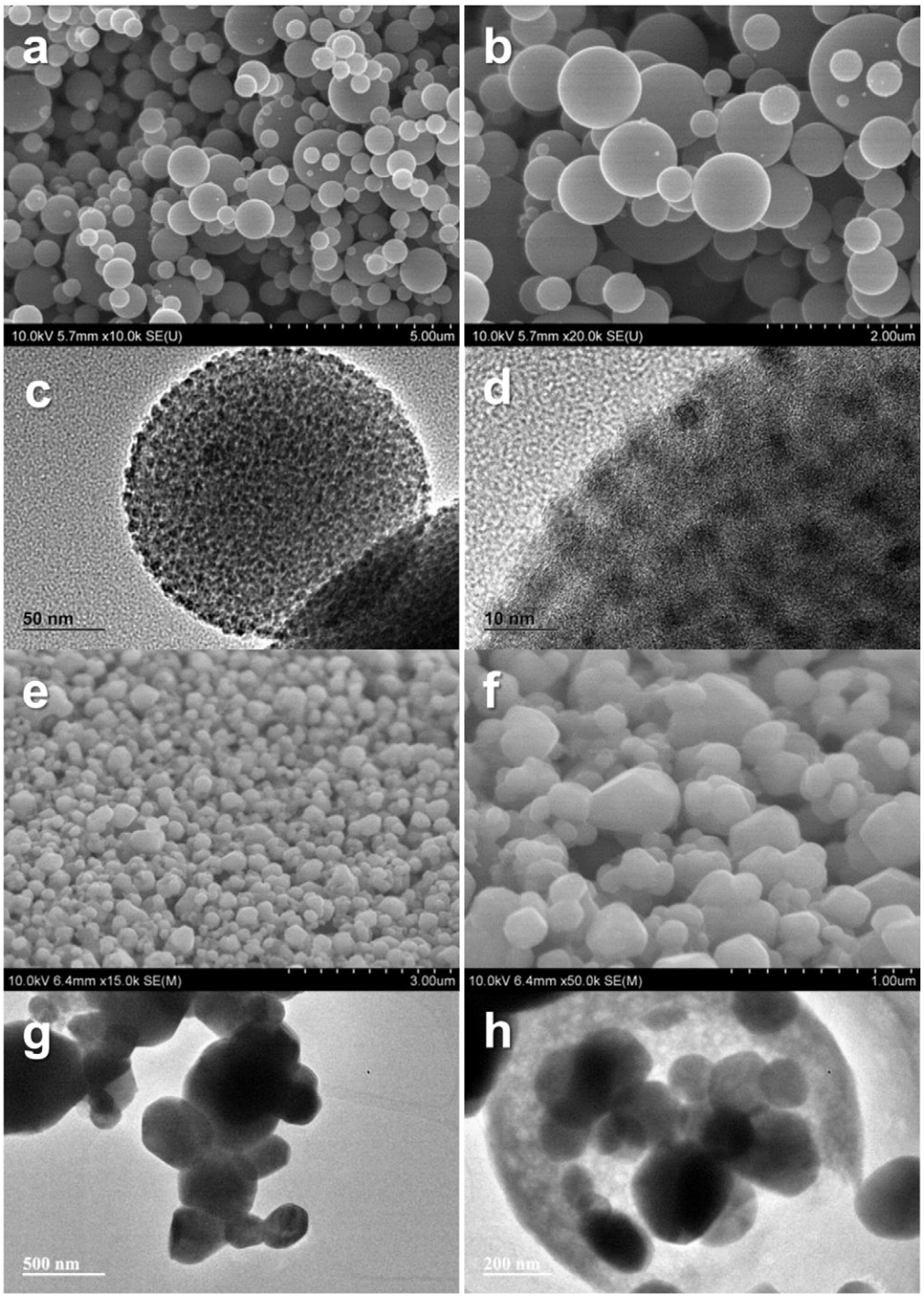

Fig. 2. (a, b) SEM and (c, d) TEM images of as-sprayed Fe_3O_4/carbon composite. (e, f) SEM and (g, h) TEM images of obtained FeS_2.

aggregation of FeS_2 particles during sulfidation reaction. The particle size of FeS_2 in present study is smaller than that of FeS_2 prepared via mechanical alloying/ball-milling [16,17]. Occasionally, FeS_2 particles encapsulated in carbon shell can be observed during the TEM imaging (Fig. 2h), implying that the mesoporous structure of as-sprayed Fe_3O_4/carbon indeed collapses during the sulfidation reaction.

The electrochemical performance of FeS_2 half-cell with sodium metal as the counter electrode and 1.0 M $NaCF_3SO_3$ in diglyme as the electrolyte is tested at 20 mA/g. As shown in Fig. 3a, the first sodiation curve is composed of a long plateau around ~1.2 V followed by a sloped line to 0.6 V. The first sodiation capacity is ~670 mAh/g, corresponding to 75% of the theoretical capacity of FeS_2 (894 mAh/g). Subsequent sodiation profiles show no voltage plateau but sloped shape with higher sodiation voltages in the capacity range of 0–270 mAh/g, considerably different with the first sodiation curve. Recent studies have pointed out that FeS_2 could not be recovered at the end of the first desodiation and a new phase of Na_xFeS_2 was discovered [19], which might account for the observed difference between the first and subsequent sodiation profiles. As suggested by Shadike et al. [19], after the 1st sodiation, the subsequent reversible sodiation–desodiation reaction between FeS_2 and sodium proceeded as following:

$$(4-x)Na^+ + (4-x)e^- + Na_xFeS_2 \leftrightarrow 2Na_2S + Fe. \quad (1)$$

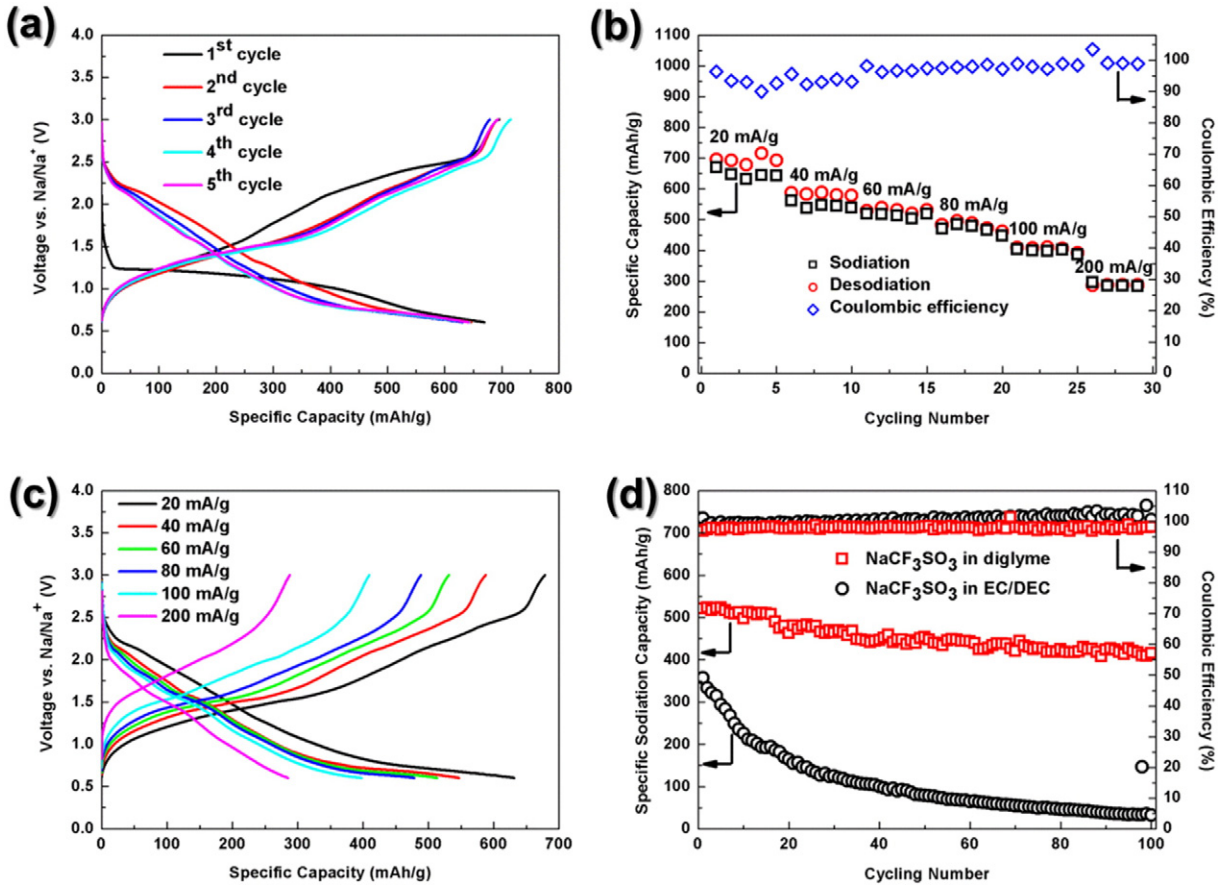

Fig. 3. (a) Initial five sodiation–desodiation voltage profiles of Na/FeS_2 cell tested in 1.0 M $NaCF_3SO_3$ in diglyme at a current density of 20 mA/g. (b) Sodiation–desodiation capacity and (c) voltage profiles of Na/FeS_2 cycled at various current densities in 1.0 M $NaCF_3SO_3$ in diglyme. (d) Cycling performance of Na/FeS_2 tested in ether- and carbonate-based electrolytes at 60 mA/g.

The first desodiation profile consists of a sloped curve during the whole process with a capacity of 690 mAh/g. The desodiation profiles during subsequent cycles present similar shape as the first one but lower polarization in the voltage range of 1.5–2.75 V. For the sodiation profiles, the voltage in the 2nd cycle is higher than that of the subsequent cycles. The observed polarization difference between the 1st/2nd cycle and subsequent cycles is probably due to the activation process during the initial few cycles. From the 1st to the 5th cycle, the sodiation and desodiation capacities vary slightly, indicating that the sodiation–desodiation reaction is highly reversible. Although the sodiation voltage of FeS_2 is lower in comparing with intercalation-type cathodes, the Na/FeS_2 system can provide a discharge energy density over 750 Wh/kg at 20 mA/g in the voltage range of 0.6–3 V, much higher than that of intercalation-type materials [9]. The rate capability of Na/FeS_2 system with 1.0 M $NaCF_3SO_3$ in diglyme electrolyte is shown in Fig. 3b with the corresponding sodiation–desodiation profiles plotted in Fig. 3c. The Na/FeS_2 system can deliver reversible sodiation capacities of 640, 550, 530, 480, 400, and 290 mAh/g at the current densities of 20, 40, 60, 80, 100, and 200 mA/g. The cycling performance of Na/FeS_2 system with 1.0 M $NaCF_3SO_3$ in diglyme electrolyte is tested at 60 mA/g and the result is shown in Fig. 3d. For comparison, the cycling performance of the same FeS_2 electrode in carbonate-based electrolyte (1.0 M $NaCF_3SO_3$ in EC/DEC, 1:1 by volume) under the same current density is also tested. The Na/FeS_2 cell tested in carbonate-based electrolyte can provide an initial sodiation capacity of 350 mAh/g. However, the capacity rapidly dropped to less than 40 mAh/g after 100 cycles, similar to the results reported for Na/FeS_2 system in the literature [16,17]. On the contrary, the Na/FeS_2 cell tested in the electrolyte of 1.0 M $NaCF_3SO_3$ in diglyme demonstrates a high initial sodiation capacity of 530 mAh/g and surprisingly good cyclability with capacity retention of 415 mAh/g after 100 cycles and Coulombic efficiency (~sodiation capacity/desodiation capacity) over 98% during the whole test, which are much better than the same system tested in carbonate-based electrolyte and the Na/FeS_2 system reported in the literature [16,17]. The improved electrochemical performance of Na/FeS_2 in ether-based electrolyte might be attributed to two factors. First, the application of ether-based electrolyte suppresses the reactions between possible sodium polysulfide and electrolyte. Second, the electrolyte of 1.0 M $NaCF_3SO_3$ in diglyme avoids the repeated formation and breaking of solid electrolyte interphase (SEI) film since this electrolyte has been shown to be stable in the voltage range of 0.01–3 V (vs. Na/Na^+) [22].

4. Conclusion

In summary, we demonstrate that by simply selecting ether-based electrolyte (1.0 M $NaCF_3SO_3$ in diglyme), the cycling performance of Na/FeS_2 system can be greatly improved in comparing with the same system tested in carbonate-based electrolyte (1.0 M $NaCF_3SO_3$ in EC/DEC). In ether-based electrolyte, the sodium storage capacity in FeS_2 can be over 600 mAh/g with a discharge energy density higher than 750 Wh/kg at 20 mA/g. The Na/FeS_2 cell can be reversibly cycled with sodiation capacity retention of 415 mAh/g after 100 cycles at 60 mA/g. The excellent sodium storage performance and cheap raw materials suggest that Na/FeS_2 system could be a very promising low cost energy storage system as long as the safety issue on the metal anode can be solved in the future. The next step of this work would be the investigation of the exact mechanisms accounting for the significantly improved electrochemical performance of Na/FeS_2 system in ether-based electrolyte.

Conflict of interest

The authors declare no conflict of interests.

Acknowledgments

The authors acknowledge the financial support of the Army Research Lab under Contract No. W911NF1420031 and the technical support of the NanoCenter at the University of Maryland.

References

[1] H. Pan, Y.-S. Hu, L. Chen, Room-temperature stationary sodium-ion batteries for large-scale electric energy storage, Energy Environ. Sci. 6 (8) (2013) 2338–2360. http://dx.doi.org/10.1039/c3ee40847g.
[2] N. Yabuuchi, K. Kubota, M. Dahbi, S. Komaba, Research development on sodium-ion batteries, Chem. Rev. 114 (23) (Dec 10 2014) 11636–11682. http://dx.doi.org/10.1021/cr500192f.PMID:25390643.
[3] Y. Xu, Y. Zhu, Y. Liu, C. Wang, Electrochemical performance of porous carbon/tin composite anodes for sodium-ion and lithium-ion batteries, Adv. Energy Mater. 3 (1) (2013) 128–133. http://dx.doi.org/10.1002/aenm.201200346.
[4] Y. Liu, Y. Xu, Y. Zhu, J.N. Culver, C.A. Lundgren, K. Xu, C. Wang, Tin-coated viral nanoforests as sodium-ion battery anodes, ACS Nano 7 (4) (Apr 23 2013) 3627–3634. http://dx.doi.org/10.1021/nn400601y.PMID:23484633.
[5] J. Qian, Y. Chen, L. Wu, Y. Cao, X. Ai, H. Yang, High capacity Na-storage and superior cyclability of nanocomposite Sb/C anode for Na-ion batteries, Chem. Commun. 48 (56) (Jul. 18 2012) 7070–7072. http://dx.doi.org/10.1039/c2cc32730a.PMID:22684188.
[6] Y. Zhu, X. Han, Y. Xu, Y. Liu, S. Zheng, K. Xu, L. Hu, C. Wang, Electrospun Sb/C fibers for a stable and fast sodium-ion battery anode, ACS Nano 7 (7) (Jul 23 2013) 6378–6386. http://dx.doi.org/10.1021/nn4025674.PMID:23802576.
[7] Y. Kim, Y. Park, A. Choi, N.S. Choi, J. Kim, J. Lee, J.H. Ryu, S.M. Oh, K.T. Lee, An amorphous red phosphorus/carbon composite as a promising anode material for sodium ion batteries, Adv. Mater. 25 (22) (Jun. 11 2013) 3045–3049. http://dx.doi.org/10.1002/adma.201204877.PMID:23494991.
[8] J. Qian, X. Wu, Y. Cao, X. Ai, H. Yang, High capacity and rate capability of amorphous phosphorus for sodium ion batteries, Angew. Chem. Int. Ed. 52 (17) (Apr. 22 2013) 4633–4636. http://dx.doi.org/10.1002/anie.201209689.PMID:23512686.
[9] N. Yabuuchi, M. Kajiyama, J. Iwatate, H. Nishikawa, S. Hitomi, R. Okuyama, R. Usui, Y. Yamada, S. Komaba, P2-type Na(x)[Fe(1/2)Mn(1/2)]O2 made from earth-abundant elements for rechargeable Na batteries, Nat. Mater. 11 (6) (Jun 2012) 512–517. http://dx.doi.org/10.1038/nmat3309. PMID:22543301.
[10] E. Bucher, Solar cell materials and their basic parameters, Applied Physics 17 (1) (1978) 1–26. http://dx.doi.org/10.1007/BF00885025.
[11] Y. Shao-Horn, S. Osmialowski, Q.C. Horn, Nano-FeS_2 for commercial Li/FeS_2 primary batteries, J. Electrochem. Soc. 149 (11) (2002) A1499–A1502. http://dx.doi.org/10.1149/1.1513558.
[12] S.B. Son, T.A. Yersak, D.M. Piper, S.C. Kim, C.S. Kang, J.S. Cho, S.S. Suh, Y.U. Kim, K.H. Oh, S.H. Lee, A stabilized PAN-FeS_2 cathode with an EC/DEC liquid electrolyte, Adv. Energy Mater. 4 (3) (2014)http://dx.doi.org/10.1002/aenm.201300961 n/a.
[13] J. Liu, Y. Wen, Y. Wang, P.A. van Aken, J. Maier, Y. Yu, Carbon-encapsulated pyrite as stable and earth-abundant high energy cathode material for rechargeable lithium batteries, Adv. Mater. 26 (Sep 10 2014) 6025–6030. http://dx.doi.org/10.1002/adma.201401496.PMID:25047510.
[14] L.L. Li, M. Cabán-Acevedo, S.N. Girard, S. Jin, High-purity iron pyrite (FeS_2) nanowires as high-capacity nanostructured cathodes for lithium-ion batteries, Nanoscale 6 (4) (Feb 21 2014) 2112–2118. http://dx.doi.org/10.1039/c3nr05851d.PMID:24441761.
[15] T. Evans, D.M. Piper, S.C. Kim, S.S. Han, V. Bhat, K.H. Oh, S.H. Lee, Ionic liquid enabled FeS_2 for high-energy-density lithium-ion batteries, Adv. Mater. 26 (43) (Nov 19 2014) 7386–7392. http://dx.doi.org/10.1002/adma.201402103.PMID:25236752.
[16] T. Kim, J. Choi, H. Ryu, G. Cho, K. Kim, J. Ahn, K. Cho, H. Ahn, Electrochemical properties of sodium/pyrite battery at room temperature, J. Power Sources 174 (2) (2007) 1275–1278. http://dx.doi.org/10.1016/j.jpowsour.2007.06.093.
[17] T. Kim, W. Jung, H. Ryu, K. Kim, J. Ahn, K. Cho, G. Cho, T. Nam, I. Ahn, H. Ahn, Electrochemical characteristics of Na/FeS_2 battery by mechanical alloying, J. Alloys Compd. 449 (1–2) (2008) 304–307. http://dx.doi.org/10.1016/j.jallcom.2006.02.113.
[18] A. Kitajou, J. Yamaguchi, S. Hara, S. Okada, Discharge/charge reaction mechanism of a pyrite-type FeS_2 cathode for sodium secondary batteries, J. Power Sources 247 (2014) 391–395. http://dx.doi.org/10.1016/j.jpowsour.2013.08.123.
[19] Z. Shadike, Y.-N. Zhou, F. Ding, L. Sang, K.-W. Nam, X.-Q. Yang, Z.-W. Fu, The new electrochemical reaction mechanism of Na/FeS_2 cell at ambient temperature, J. Power Sources 260 (2014) 72–76. http://dx.doi.org/10.1016/j.jpowsour.2014.03.011.
[20] T. Yim, M.-S. Park, J.-S. Yu, K.J. Kim, K.Y. Im, J.-H. Kim, G. Jeong, Y.N. Jo, S.-G. Woo, K.S. Kang, I. Lee, Y.-J. Kim, Effect of chemical reactivity of polysulfide toward carbonate-based electrolyte on the electrochemical performance of Li–S batteries, Electrochim. Acta 107 (2013) 454–460. http://dx.doi.org/10.1016/j.electacta.2013.06.039.
[21] Y. Xu, G. Jian, Y. Liu, Y. Zhu, M.R. Zachariah, C. Wang, Superior electrochemical performance and structure evolution of mesoporous Fe_2O_3 anodes for lithium-ion batteries, Nano Energy 3 (2014) 26–35. http://dx.doi.org/10.1016/j.nanoen.2013.10.003.
[22] B. Jache, P. Adelhelm, Use of graphite as a highly reversible electrode with superior cycle life for sodium-ion batteries by making use of co-intercalation phenomena, Angew. Chem. Int. Ed. 53 (38) (Sep 15 2014) 10169–10173. http://dx.doi.org/10.1002/anie.201403734.PMID:25056756.